Journal of Hazardous Materials 416 (2021) 126201

Contents lists available at ScienceDirect

Journal of Hazardous Materials

journal homepage: www.elsevier.com/locate/jhazmat

Research Paper

A photoelectrochemical self-powered sensor for the detection of sarcosine based on NiO NSs/PbS/Au NPs as photocathodic material

Hanyu Wang [a,b], Yanting Qi [a,b], Dan Wu [a,b,*], Qin Wei [a,b]

[a] Collaborative Innovation Center for Green Chemical Manufacturing and Accurate Detection, School of Chemistry and Chemical Engineering, University of Jinan, Jinan 250022, PR China

[b] Key Laboratory of Interfacial Reaction & Sensing Analysis in Universities of Shandong, School of Chemistry and Chemical Engineering, University of Jinan, Jinan 250022, PR China

ARTICLE INFO

Editor: Dr. L. Haizhou

Keywords:
PEC self-powered cathodic sensor
Sarcosine
NiO/PbS/Au nanomaterial
High PEC activity

ABSTRACT

In this study, lead(II) sulfide (PbS) nanocrystals were modified on nickel(II)oxide nanosheets (NiO NSs) via the chemical bath method. Afterwards, Au nanoparticles (NPs) were also modified successfully. A photoelectrochemical (PEC) self-powered platform for detecting sarcosine with high PEC activity was constructed. The capacity of NiO NSs to be loaded with other sensitizing materials was mainly attributed to its porous structure and large specific surface area. Under optimum conditions, the constructed PEC self-powered cathodic sensor for detecting sarcosine exhibited a linear range in 5.0×10^{-8}–5.0×10^{-2} mol/L with a detection limit (LOD) of 1.7×10^{-8} mol/L. The biosensor demonstrated good reproducibility, acceptable stability and high specificity, thus confirming its potential application in the detection of other similar substances.

1. Introduction

Sarcosine is formed by the methylation of glycine and it exists in the human body in trace amounts. Sarcosinemia and other diseases, including prostate cancer can be caused by an extremely high concentration of sarcosine in the plasma or urine. It has been reported that sarcosine, which is also known as N-methylglycine can effectively reflect the severity of prostate cancer and reveal the growth behaviors (slowly growing or highly invasive) of cancer cells (Sreekumar et al., 2009). Further, urinary creatine detection is a more accurate method of diagnosing prostate cancer compared with the detection of blood prostate-specific antigen that is commonly adopted in the clinic (Khan et al., 2018; Wang et al., 2019). Thus, it is particularly valuable to achieve the rapid and sensitive detection of sarcosine.

In recent years, much effort has been invested into developing sensors, such as self-powered biosensors (Dong et al., 2020; Yao et al., 2020; Tong et al., 2021; Zhong et al., 2021; Zhu et al., 2021; Peng et al., 2014). Li et al. integrated an enzymatic biofuel cell (EBFC) with the deoxyribonucleic acid (DNA) amplification strategy to design a self-powered biosensor for detecting SNPs (Gu et al., 2019). Generally, a typical self-powered biosensing platform does not require an external power and bias (Tang et al., 2019; Chen et al., 2019; Gai et al., 2017, 2018; Peng et al., 2021; Zhao et al., 2017). Its power can be directly supplied by the sensor to act on the sensing device, thus affording the sensor with a good prospect in immunoassay (Huang et al., 2020; Ouyang et al., 2020; Guan et al., 2019; Zeng et al., 2018; Chen et al., 2017). Furthermore, the PEC self-powered biosensor exhibited advantages, such as economic efficiency, facile operation, portability and miniaturization. Thus, it exhibited good application prospects in the fields of no-battery devices (Yang et al., 2019; Zhu et al., 2020; Peng et al., 2018).

Semiconductor materials are generally divided into n-type and p-type semiconductors. Compared with n-type semiconductors, the p-type ones exhibit stronger anti-interference and anti-reduction abilities (Zhang et al., 2018; Zhu et al., 2019; Han et al., 2021), which is mainly because of their stronger resistance to oxidation (Gao et al., 2014; Chuang et al., 2014). Moreover, the reducing substances, such as ascorbic acid and glutathione, in electrolytes may greatly impact the n-type semiconductors. Therefore, many p-type semiconductors were utilized in recent years to construct sensors, as well as for biological analyses. NiO, an inexpensive p-type semiconductor with a large band gap (3.5 eV), is widely utilized in the field of PEC sensing and catalysis (Huang et al., 2017; Cao et al., 2020; Hu et al., 2020). Owing to the limitation of the weak PEC signal of pure NiO, it is generally necessary to combine it with other representative semiconductors to enhance its PEC

* Corresponding author at: Collaborative Innovation Center for Green Chemical Manufacturing and Accurate Detection, School of Chemistry and Chemical Engineering, University of Jinan, Jinan 250022, PR China.
E-mail address: wudan791108@163.com (D. Wu).

https://doi.org/10.1016/j.jhazmat.2021.126201
Received 30 January 2021; Received in revised form 14 May 2021; Accepted 20 May 2021
Available online 24 May 2021

signal (Jasim et al., 2020; Xu et al., 2015; Oluwalana and Ajibade, 2020; Wu et al., 2018; Park et al., 2014). The introduction of a narrow band gap semiconductor, PbS (0.41 eV), can enhance the absorption and utilization of light energy by pure NiO, thereby improving its photoelectric conversion efficiency (Yang et al., 2018; García-Valenzuela et al., 2013; Park et al., 2015; Hou et al., 2020). Moreover, PbS exhibits excellent photoconductivity and demonstrates strong confinement of charge carriers (Khot et al., 2015; Wang et al., 2019).

In this work, a PEC self-powered sensor, which was designed with a narrow band gap semiconductor, NiO NSs, as the base material, was constructed via layer-by-layer modification. In detail, nickel(II)hydroxide ($Ni(OH)_2$) was calcined at a specific temperature to convert it into NiO, which adheres tightly to the working electrode. Following the successive modifications of the PbS nanocrystals, as well as Au NPs, the NiO/PbS/Au composite nanomaterial with improved PEC response was formed. This combination strategy can adequately utilize light energy and efficiently promote charge separation, thus improving the photocurrent conversion efficiency. As shown in Scheme 1, a good detection of sarcosine was achieved after sarcosine oxidase (SOx) was immobilized on the electrode. Furthermore, the constructed sensor exhibited a signal-suppression mechanism, which depended on O_2. Compared with the biosensors in similar studies, the PEC biosensor in this study exhibited good performance owing to the unique nanostructure of NiO/PbS/Au NPs, as well as the good electrical conductivity and surface plasmon resonance (SPR) effect of Au NPs (Lv et al., 2020). Therefore, the unique combination of materials, as well as an appropriate structural design, greatly improved the performance of the PEC biosensors.

2. Experimental part

2.1. Materials and instruments

Nickel(II)nitrate hexahydrate ($Ni(NO_3)_2{\cdot}6H_2O$) was obtained from Guangcheng Chemical Reagent Factory. Potassium persulfate ($K_2S_2O_8$) and gold chloride tetrahydrate ($HAuCl_4{\cdot}4H_2O$) were purchased from Sinopharm Chemical Reagent Co., Ltd. (Shanghai, China). Aqueous ammonia (25–28%) was obtained from Tianjin Fuyu Fine Chemical Co., Ltd (Tianjin, China). Lead(II)nitrate ($Pb(NO_3)_2$) was purchased from Macklin Biochemical Co., Ltd. (Shanghai, China). Ethylene glycol was obtained from Tianjin Damao Chemical Reagent Factory. Polydiallyl dimethylammonium chloride (PDDA) was purchased from Aladdin Industrial Corporation (Shanghai, China). The indium-tin oxide (ITO) was purchased from China Southern Glass Holding Co., Ltd (Shenzhen, China). All the reactants were analytically pure and were utilized, as received.

The electrochemical impedance spectroscopy (EIS) was measured on a Zahner Zennium electrochemical workstation (PP211, Germany). X-ray powder diffraction (XRD) analysis was performed on a D8 Advance X-ray diffractometer (Bruker AXS, Germany) in the range of 10–80° (2θ). Scanning electron microscopy (SEM) and element mapping were performed on a field-emission scanning electron microscope (Zeiss Gemini SEM 300, GER). High-resolution transmission electron microscopy (HRTEM) was performed with a JEM-2100 electron microscope (JEOL, Japan). The ultraviolet-visible (UV–Vis) diffuse reflectance light spectra were measured on a UV–Vis spectrophotometer (TU-1901, Beijing Purkinje General Instrument Co Ltd.,). The PEC measurement was conducted on an electrochemical workstation (IVIUM Vertex One, Netherlands).

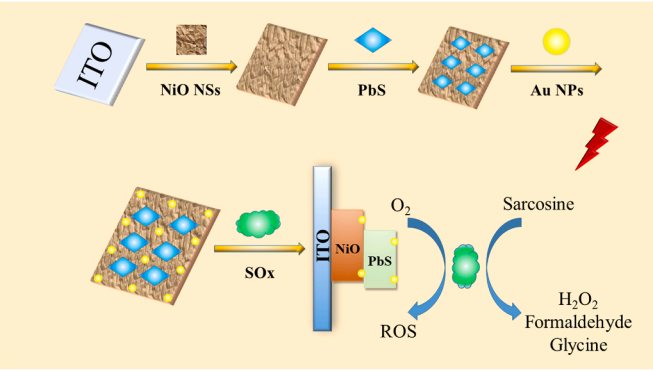

Scheme 1. Fabrication of the PEC self-powered photocathodic biosensor for detecting sarcosine.

2.2. Synthesis of ITO/NiO/PbS

To ensure the progress of the experiment, the ITO conductive glass substrate was pretreated before utilization. The ITO conductive glass substrate was cut into 1 × 2 cm^2 and placed in a solution of washing powder, 1 mol/L NaOH, ethanol and ultrapure water every 20 min. The treated ITO conductive substrate was blown dry with nitrogen to prepare it for the subsequent step. A facile method was employed to grow $Ni(OH)_2$ NSs. Further, 1.23 g of $Ni(NO_3)_2{\cdot}6H_2O$ was dissolved in 35 mL of ultrapure water, after which 0.2 g of $K_2S_2O_8$ was added and stirred. Thereafter, 5 mL of concentrated aqueous ammonia (25–28%) was added to prepare the precursor solution. The mixture solution was transferred into a Teflon-lined steel autoclave (50 mL) after 10 min of stirring. A piece of the ITO glass substrate was placed with the conductive surface facing downwards and maintained for 10 h at 150 °C. This approach facilitated the growth of a green $Ni(OH)_2$ array film on the ITO. The film was calcined for 2 h at 400 °C to form a dark-yellow NiO NSs.

Furthermore, ITO/NiO/PbS was synthesized employing ITO/NiO via the chemical bath method. Briefly, ITO/NiO was immersed in a 0.1 mol/L $Pb(NO_3)_2$ methanol solution to ensure that sufficient Pb^{2+} ions were absorbed on the surface of the substrate. Afterwards, they were rinsed with an anhydrous methanol solution for 1 min to remove the unsteadily bound excess Pb^{2+}. Thereafter, ITO/NiO was dipped into a 0.1 mol/L Na_2S methanol solution in which the adsorbed Pb^{2+} reacted with S^{2-} for 30 s to form a thin layer of PbS. Afterwards, the electrode was rinsed with an anhydrous methanol solution for 1 min

2.3. Fabrication of the PEC self-powered biosensor

The proposed sensor was constructed according to previous reports but with minor modifications (Shi et al., 2018). In the first step, the 2% PDDA solution was prepared and ITO/NiO/PbS/Au electrode was dipped in the aforementioned solution containing 0.5 mol/L NaCl. Secondly, it was allowed to stand for 2 h at room temperature to generate adhesion (Song et al., 2018). Next, 10 μL of 0.5 mg/mL SOx was dropped on the above proposed electrode to initiate a connection with PDDA and achieve a specific recognition with sarcosine. Subsequently, it was incubated in the refrigerator for 2 h at 4 °C.

2.4. PEC measurement of sarcosine

The PEC analysis of the proposed biosensor was performed in a 0.1 mol/L Tris-HCl solution (pH = 7.0). The photocurrent was measured via the chronoamperometry (i-t) method. The light source was a flexible wavelength scope of 420–430 nm, and the bias voltage was 0 V. The three-electrode pattern was adopted for the PEC measurement. A slide of the modified ITO electrode was utilized as the working electrode, and a Pt wire and saturated calomel electrode were employed as the counter and reference electrodes, respectively.

3. Results and discussion

3.1. Characterization of the materials

NiO was produced by calcining $Ni(OH)_2$ for 2 h at 450 °C. Fig. 1A and 1B showed the TEM and SEM images of NiO, respectively. The lamella structure of NiO was observed from the TEM image, thereby confirming the existence of NiO. Fig. 1B and the inset showed the different magnifications of the SEM images of NiO. The thickness was ~200 nm. It could be observed that NiO exhibited an ordered nanoarray structure, which benefitted the loading of other substances. Further, the TEM and SEM images confirmed that NiO exhibited a nanosheet array structure. Furthermore, XRD, which is a valuable method of analyzing substances, is generally employed to define certain substances. The XRD patterns of the NiO (black line) and NiO/PbS composites (red line) were obtained, as shown in Fig. 1C. NiO NSs exhibited sharp diffraction peaks at 37°, 43°, 62°, 75° and 79°, which corresponded to the (111), (200), (220), (311) and (222) crystal forms, respectively. This result revealed the formation of NiO (JCPDS PDF#47-1049) and the absence of other Ni-related impurities in the sample. Regarding NiO/PbS, in addition to the peak position of NiO, strong diffraction peaks, which corresponded to (111), (200), (220), (311), (222) and (400), appeared at 26°, 30°, 43°, 50°, 53° and 63°, thereby confirming the successful loading of PbS (JCPDS PDF#05-0592) on NiO (Zhu et al., 2019; Suganya and Balu, 2017). Fig. 1D showed the SEM image of the NiO/PbS composite. It can be seen that PbS exhibited a small nanocrystalline shape and was tightly coupled to the NiO NSs array, thereby availing additional sites for loading SOx. Further, Fig. 1E showed the element mapping of the NiO/PbS composite. It revealed that elements O and Ni, as well as S and Pb, were approximately in the same distribution position, further verifying the modification of PbS on the porous NiO NSs. Fig. 1F showed the spherical AuNPs on NiO/PbS. After forming Au–S bonds between Au with PbS, the material exhibited a loose and porous shape, which proved the recombination of AuNPs.

3.2. Characterization of the modified electrode

Fig. 2(A) showed the HRTEM image of AuNPs with a diameter of 14–16 nm (Fig. 2(A) inset). The UV–Vis absorption diffuse reflectance spectra of NiO (black), NiO/PbS (red) and NiO/PbS/Au (blue) were also measured. Fig. 2B showed that the bare NiO electrode barely absorbed visible light mainly because of the relatively broad excitation of its band gap. Significant absorption of NiO/PbS was observed above 400 nm. Regarding the NiO/PbS/Au composites, the absorption rate further increased in the same wavelength range. Under visible light irradiation, the continuous increase in the absorption rate further indicated that the prepared NiO/PbS/Au electrode was suitable to be utilized as a photosensitive electrode. Additionally, the appearance of the NiO/PbS/Au peak at 560 nm might be due to the SPR effect of AuNPs.

Incidentally, the characteristic linear sweep voltammetry curve of the ITO/NiO/PbS/Au electrode was also measured under illumination and dark conditions, and the result was shown in the supplementary material (Fig. S1, supplementary material).

To verify the success of the layer-by-layer modification process of the biosensor, the PEC response was conducted, as well as electrochemical impedance spectroscopy (EIS). Fig. 3A showed that the value of the PEC signal of a single NiO NSs was only approximately −100 nA (curve a) under visible light irradiation (420–430 nm). Thereafter, a very significant enhancement was observed in the signal after the modification of PbS (curve b) probably because the modification had sensitized the band gap of NiO and increased its absorbance. The value of the photocurrent was continuously increased as AuNPs were further coated on the electrode. AuNPs materials generally exhibited good electrical conductivity. Additionally, they exert unique SPR effects. These unique characteristics accounted for the increase in the photocurrent value to −6 μA. After loading SOx (curve d), the photocurrent became lower than that of NiO/PbS/Au probably because SOx prevented the material from absorbing visible light. Fig. 3B showed the EIS result of the constructed PEC self-powered biosensor, and the curve in the figure corresponded to that in Fig. 3A. The EIS semicircle represented R_{et}. The plot revealed that R_{et} of bare ITO was smaller than that of ITO/NiO, thus indicating that NiO NSs were loaded. Compared with the red curve, R_{et} of the blue curve was much higher than that of the former. This might be due to the modification of p-type PbS, which increased the electron-transfer resistance. Following the modification of AuNPs (green curve), R_{et} of that diminished and this could be attributed to the outstanding electrical

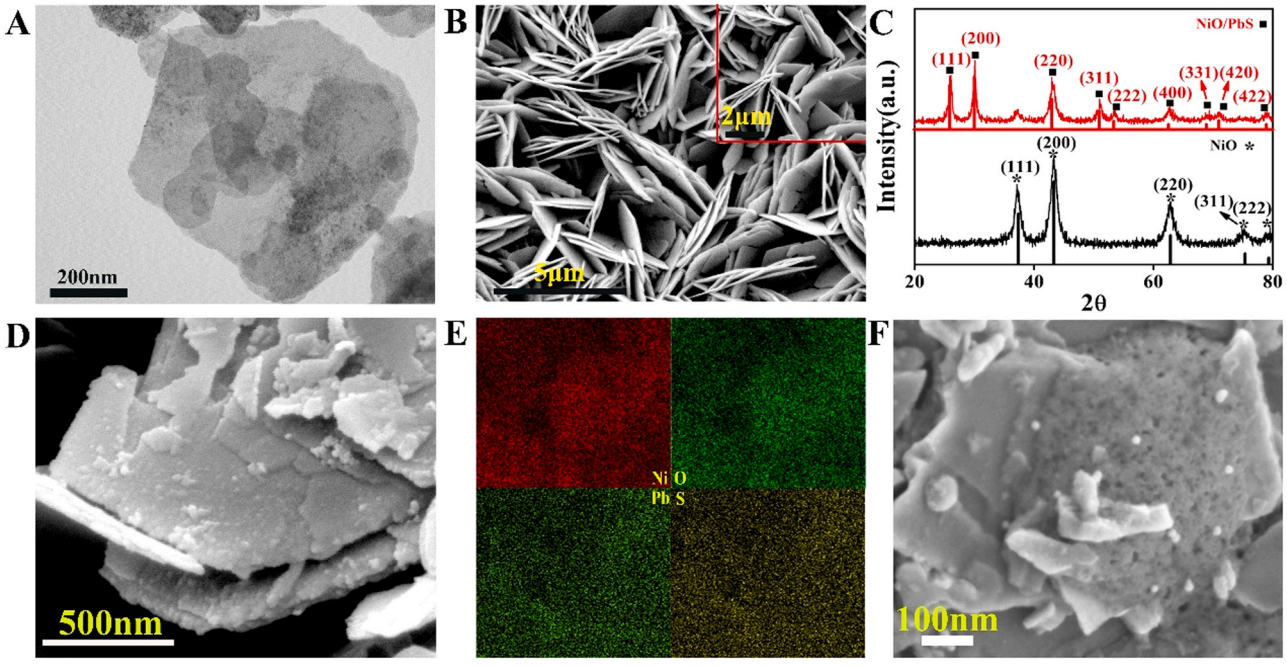

Fig. 1. (A) TEM image of NiO NSs, (B) SEM image of NiO with a 5 μm scale (the inset is the SEM image of NiO NSs with the scale of 2 μm), (C) XRD patterns of the as-synthesized NiO NSs and NiO/PbS compounds, (D) SEM image and (E) element mappings of the NiO/PbS compounds, and (F) SEM image of NiO/PbS/Au.

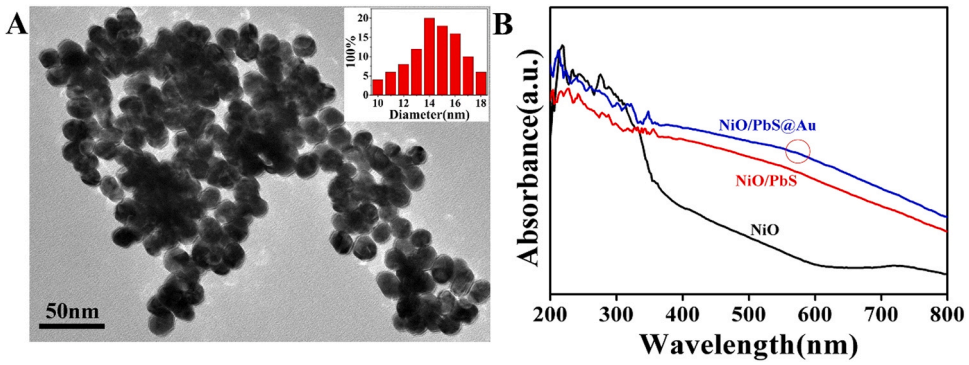

Fig. 2. (A) HRTEM of AuNPs (inset: AuNPs size distribution), (B) UV–Vis absorption diffuse reflectance spectra of the as-synthesized NiO, NiO/PbS and NiO/PbS/Au.

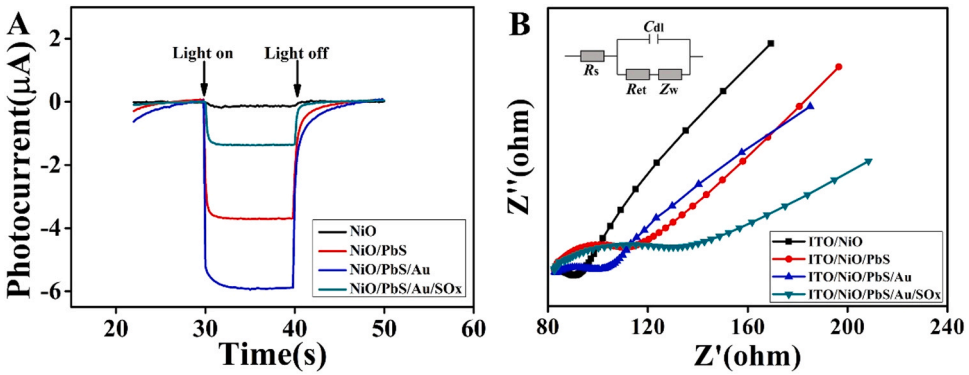

Fig. 3. (A) PEC response and (B) corresponding electrochemical impedance spectroscopy (EIS) Nyquist plots (tested in 0.1 and 2.5 mmol/L KCl and $Fe(CN)_6^{3-/4-}$, respectively) of the prepared electrode. The inset in (B) shows the EIS equivalent circuit.

conductivity. When SOx was fixed on the surface of the ITO/NiO/PbS/Au electrode (pink curve), it further increased R_{et} probably because of the hindrance of the protein.

3.3. Possible electron-transfer mechanism of the constructed biosensor

As shown in Scheme 2, the photo-generated electrons of the photocathode reacted with O_2 in the electrolyte to form O_2^- under visible light irradiation. Further, AuNPs exerted a unique SPR effect and simultaneously availed electrons to the conduction bands of PbS and NiO, further improving the PEC performance of the NiO/PbS electrode. Moreover, the good electrical conductivity of AuNPs contributed to the acceleration of the electron transmission. What is more, the SOx decomposition of sarcosine consumed O_2 to form H_2O_2 and other substances. After modifying SOx, the cathodic PEC performance of the self-powered sensor diminished mainly because of the competition between SOx and NiO/PbS/Au to consume O_2.

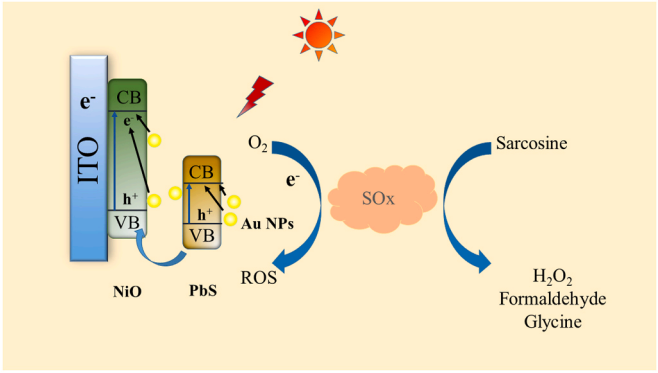

Scheme 2. Electron-transfer mechanism of the proposed biosensor.

3.4. Selection of the best experimental conditions

The experimental conditions were explored to obtain the maximum photocurrent value from the PEC measurement. The specific experimental conditions were shown in Fig. S2.

3.5. PEC analysis of the constructed self-powered sensor

In order to explore the performance of the NiO/PbS/Au photocathode in dissolving oxygen, comparative tests were conducted in different environments (Fig. 4A). O_2 can be consumed by SOx via the oxidation of sarcosine to yield H_2O_2, formaldehyde and glycine. Next, 1 mmol/L H_2O_2 was added to the buffer solution with saturated N_2, as shown by the red curve. Compared with the PEC response of the N_2-saturated buffer solution without H_2O_2 (black curve), no significant change was observed. The electrode achieved the highest photocurrent in the air-saturated buffer solution (blue curve). These results were consistent with those of previous studies and indicated that the effect of the dissolved O_2 on the cathodic photocurrent was greater than that of H_2O_2 on the proposed PEC enzyme biosensing system. Under the selected test conditions, Fig. 4B described that the photocurrent diminished regularly as the concentration of sarcosine increased. As the concentration of sarcosine increased, the competition between the photocathode and SOx was also intensified. Put differently, as the concentration of sarcosine increased, the dissolved oxygen, as an electron acceptor, was readily consumed by SOx. Fig. 4C showed that in the range of 5.0×10^{-8}–5.0×10^{-2} mol/L, the photocurrent response exhibited a linear decrease as the logarithm of the concentration of sarcosine increased. Compared with the other reports on the detection of sarcosine, which were many, the constructed biosensor exhibited a

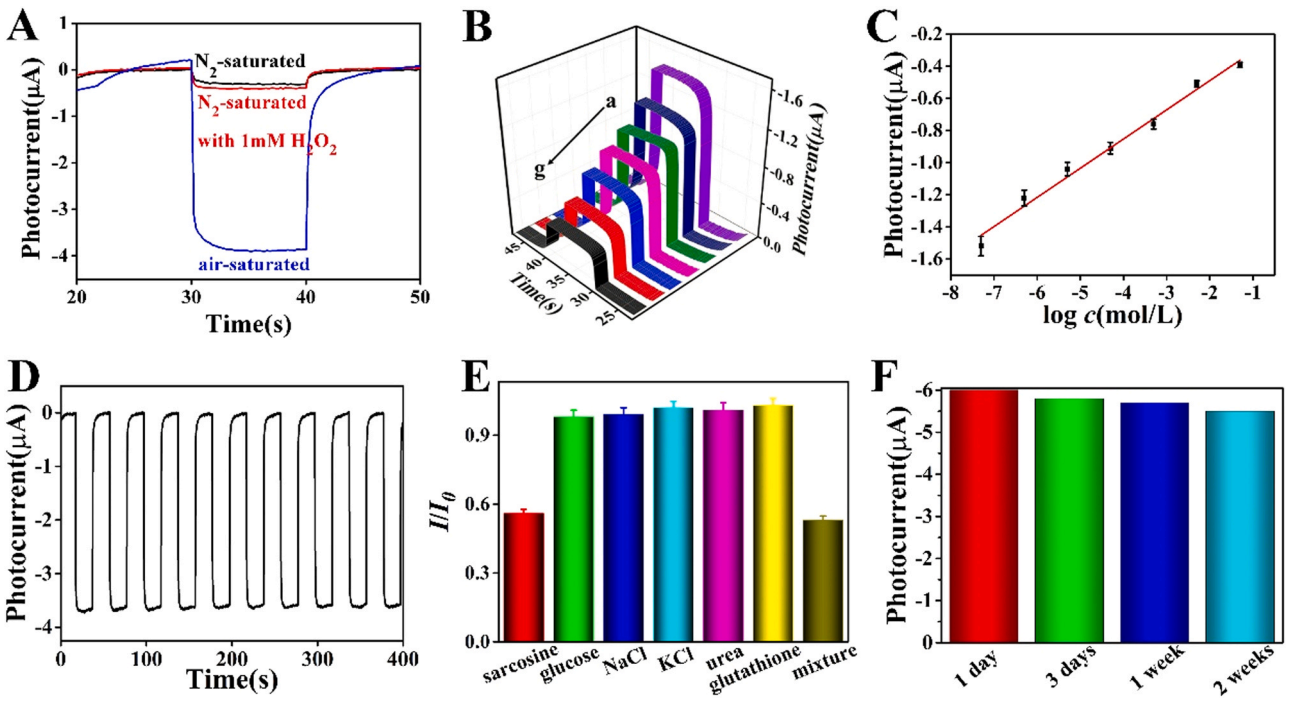

Fig. 4. (A) PEC performance of air-saturated ITO/NiO/PbS/Au (blue curve) and deoxygenation by N_2 before (black curve) and after (red curve) the addition of 1 mmol/L H_2O_2 (0.1 mol/L Tris-HCl solution prepared with 0 V voltage), (B) PEC responses of the SOx modified electrode corresponding to different sarcosine concentrations (from curves a to g (5.0×10^{-8}–5.0×10^{-2} mol/L)), (C) Photocurrent values of SOx modified with different sarcosine concentrations vs log *c*, (D) PEC responses of the ITO/NiO/PbS/Au electrode after several 'light on–light off–light on' cycles for 400 s with an applied voltage of 0 V. (E) Specificity of the proposed biosensor. *I* and I_0 are the photocurrent responses before and after the addition of the interfering substance, respectively. (F) Storage stability of the proposed biosensor. For interpretation of the references to color in this figure legend, the reader is referred to the web version of this article.

wider detection range and a lower LOD (Table S1, supplementary material). The resulting calibration equation was $I = 0.18 \log c - 0.13$, and the correlation coefficient (R) was 0.992.

3.6. Stability, specificity and reproducibility of the prepared self-powered sensor

Stability is one of the significant conditions to consider when measuring the performance of a sensor. As shown in Fig. 4D, the PEC self-powered sensor did not exhibit any significant change in the photocurrent after multiple on/off irradiation cycles for 400 s, and this demonstrated its satisfactory stability.

Further, specificity is another valuable indicator for evaluating the performance of a sensor. Thus, sarcosine (10^{-6} mol/L), glucose (1 mmol/L), NaCl (1 mmol/L), KCl (1 mmol/L), urea (1 mmol/L), glutathione (1 mmol/L) and a mixture containing all of them were selected for the test (Fig. 4E). The results indicated that there was no significant change in the photocurrent before and after the additions of glucose, NaCl, KCl, urea and glutathione, thereby confirming that the biosensor exhibited excellent specificity for sarcosine. Furthermore, storage stability is another valuable indicator for measuring the performance of a sensor. Thus, we tested the storage stability of the prepared sensor (Fig. 4F). The PEC performances of the prepared electrode were tested on the first and third days, as well as on the first and second weeks. The test results revealed that the detected photocurrent response was −6 μA on the first day. The photocurrent response after two weeks was −5.5 μA, which is 91.7% that of the first day, further indicating good storage stability. Intra-assays and inter-assays were employed to test the repeatability of this PEC self-powered biosensor. The prepared ITO/NiO/PbS/Au electrode was measured five times in a 5.0×10^{-7} mol/L solution for the intra-assay test, and the RSD of 4.9% was obtained. Under the same conditions, five ITO/NiO/PbS/Au electrodes were measured in the 5.0×10^{-7} mol/L solution for the inter-assay measurement, and the RSD value of 4.3% was obtained. The results indicated that the PEC self-powered sensor exhibited good reproducibility.

3.7. Actual sample analysis

To further explore the practicability of the designed biosensor, the standard addition method was employed (Park et al., 2014). Different concentrations of sarcosine (5.0×10^{-7}, 5.0×10^{-5} and 5.0×10^{-3} mol/L) were added to a real sample. Table S2 revealed that RSD was from 1.2% to 3.8% and that the recovery rate was from 98.2% to 106%. The RSD and recovery results confirmed that the constructed biosensor exhibited good accuracy and precision.

4. Conclusion

Briefly, a unique PEC self-powered biosensing platform was established employing NiO/PbS/Au NPs as the photocathodic material. The characterization of the nanocomposites, as well as the construction of the sensors, were described. The experimental results indicated that AuNPs, PbS nanocrystals and NiO NSs were ideally coupled. Owing to the sensitization of PbS and the SPR effect and good electrical conductivity of AuNPs, the constructed PEC self-powered sensor exhibited excellent sensitivity to O_2 and good PEC performance. More significantly, these advantages confirmed that the self-powered biosensors could be employed to detect sarcosine in human serum samples. It is hoped that these new sensor platforms would be further integrated with advanced materials and microfabrication technologies in the future to diagnose diseases and perform clinical analyses.

CRediT authorship contribution statement

Hanyu Wang: Writing - original draft, Data curation. **Yanting Qi:**

Investigation, Experimental guidance. **Dan Wu:** Writing guidance, Supervision, Writing - review & editing. **Qin Wei:** Formal analysis, Experimental support.

Declaration of Competing Interest

The authors declare that they have no known competing financial interests or personal relationships that could have appeared to influence the work reported in this paper.

Acknowledgements

We gratefully acknowledge the financial support of the Young Taishan Scholars Program of Shandong Province (tsqn201909124), the National Natural Science Foundation of China (21775054), the Project of "20 items of University" of Jinan (2019GXRC018) and the National Key Scientific Instrument and Equipment Development Project of China (21627809). All the authors express their sincere thanks.

Appendix A. Supporting information

Supplementary data associated with this article can be found in the online version at doi:10.1016/j.jhazmat.2021.126201.

References

Cao, R., Xu, J., Shi, S., Chen, J., Liu, D., Bu, Y., Zhang, X., Yin, S., Li, L., 2020. High-performance self-powered ultraviolet photodetectors based on mixed-dimensional heterostructure arrays formed from NiO nanosheets and TiO_2 nanorods. J. Mater. Chem. C 8, 9646–9654.

Chen, C., Xi, J., Zhou, E., Peng, L., Chen, Z., Gao, C., 2017. Porous graphene microflowers for high-performance microwave absorption. Nanomicro Lett. 10, 26.

Chen, K., Wang, S., He, C., Zhu, H., Zhao, H., Guo, D., Chen, Z., Shen, J., Li, P., Liu, A., Li, C., Wu, F., Tang, W., 2019. Photoelectrochemical self-powered solar-blind photodetectors based on Ga_2O_3 nanorod array/electrolyte solid/liquid heterojunctions with a large separation interface of photogenerated carriers. ACS Appl. Nano Mater. 2, 6169–6177.

Chuang, S., Battaglia, C., Azcatl, A., McDonnell, S., Kang, J., Yin, X., Tosun, M., Kapadia, R., Fang, H., Wallace, R., Javey, A., 2014. MoS_2 p-type transistors and diodes enabled by high work function MoO_x contacts. Nano Lett. 14, 1337–1342.

Dong, X., Shi, Z., Xu, C., Yang, C., Chen, F., Lei, M., Wang, J., Cui, Q., 2020. CdS quantum dots/Au nanoparticles/ZnO nanowire array for self-powered photoelectrochemical detection of Escherichia coli O157:H7. Biosens. Bioelectron. 149, 111843.

Gai, P., Gu, C., Hou, T., Li, F., 2017. Ultrasensitive self-powered aptasensor based on enzyme biofuel cell and DNA bioconjugate: a facile and powerful tool for antibiotic residue detection. Anal. Chem. 89, 2163–2169.

Gai, P., Gu, C., Hou, T., Li, F., 2018. Integration of biofuel cell-based self-powered biosensing and homogeneous electrochemical strategy for ultrasensitive and easy-to-use bioassays of microRNA. ACS Appl. Mater. Interfaces 10, 9325–9331.

Gao, J., Miao, J., Li, P., Teng, W., Yang, L., Zhao, Y., Liu, B., Zhang, Q., 2014. A p-type Ti (iv)-based metal–organic framework with visible-light photo-response. Chem. Commun. 50, 3786–3788.

García-Valenzuela, J., Baez-Gaxiola, M., Sotelo-Lerma, M., 2013. Chemical bath deposition of PbS thin films on float glass substrates using a $Pb(CH_3COO)_2$–NaOH–$(NH_2)_2CS$–$N(CH_2CH_2OH)_3$–CH_3CH_2OH definite aqueous system and their structural, optical, and electrical/photoelectrical characterization. Thin Solid Films 534, 126–131.

Gu, C., Kong, X., Liu, X., Gai, P., Li, F., 2019. Enzymatic biofuel-cell-based self-powered biosensor integrated with DNA amplification strategy for ultrasensitive detection of single-nucleotide polymorphism. Anal. Chem. 91, 8697–8704.

Guan, H., Zhong, T., He, H., Zhao, T., Xing, L., Zhang, Y., Xue, X., 2019. A self-powered wearable sweat-evaporation-biosensing analyzer for building sports big data. Nano Energy 59, 754–761.

Han, Q., Zhao, X., Na, N., Ouyang, J., 2021. Integrating near-infrared visual fluorescence with a photoelectrochemical sensing system for dual readout detection of biomolecules. Anal. Chem. 93, 3486–3492.

Hou, J., Yang, Y., Zhou, J., Wang, Y., Xu, T., Wang, Q., 2020. Flexible CdS and PbS nanoparticles sensitized TiO_2 nanotube arrays lead to significantly enhanced photocatalytic performance. Ceram. Int. 46, 28785–28791.

Hu, X., Wang, G., Wang, J., Hu, Z., Su, Y., 2020. Step-scheme NiO/BiOI heterojunction photocatalyst for rhodamine photodegradation. Appl. Surf. Sci. 511, 145499.

Huang, M., Zhou, C., Tian, J., Yang, K., Yang, H., Lu, J., 2020. Self-powered aptasensing for prostate specific antigen based on a membraneless photoelectrochemical fuel cell. Biosens. Bioelectron. 165, 112357.

Huang, W., Ge, L., Chen, Y., Lai, X., Peng, J., Tu, J., Cao, Y., Li, X., 2017. $Ni(OH)_2$/NiO nanosheet with opulent active sites for high-performance glucose biosensor. Sens. Actuators B. Chem. 248, 169–177.

Jasim, M., Dakhil, O., Hussein, E., Abdullah, H., 2020. Enhanced photoelectrochemical properties of NiO nanoparticles-decorated TiO_2 nanotube arrays for water splitting. J. Mater. Sci. Mater. Electron. 31, 10707–10714.

Khan, M., Dighe, K., Wang, Z., Srivastava, I., Daza, E., Schwartz-Dual, A., Ghannam, J., Misra, S., Pan, D., 2018. Detection of prostate specific antigen (PSA) in human saliva using an ultra-sensitive nanocomposite of graphene nanoplatelets with diblock-co-polymers and Au electrodes. Analyst 143, 1094–1103.

Khot, K., Mali, S., Mane, R., Patil, P., Hong, C., Kim, J., Heo, J., Bhosale, P., 2015. Synthesis, characterization and photoelectrochemical properties of PbS sensitized vertically aligned ZnO nanorods: modified aqueous route. J. Mater. Sci. Mater. Electron. 26, 6897–6906.

Lv, S., Zhang, K., Zhou, Q., Tang, D., 2020. Plasmonic enhanced photoelectrochemical aptasensor with D-A F8BT/g-C_3N_4 heterojunction and AuNPs on a 3D-printed device. Sens. Actuators B. Chem. 310, 127874.

Oluwalana, A.E., Ajibade, P.A., 2020. Structural, optical and photocatalytic studies of oleylamine capped PbS nanoparticles. Opt. Quant. Electron. 53, 2.

Ouyang, X., Tang, L., Feng, C., Peng, B., Liu, Y., Ren, X., Zhu, X., Tan, J., Hu, X., 2020. Au/CeO_2/g-C_3N_4 heterostructures: designing a self-powered aptasensor for ultrasensitive detection of microcystin-LR by density functional theory. Biosens. Bioelectron. 164, 112328.

Park, J., Seo, J., Park, S., Shin, S., Kim, Y., Jeon, N., Shin, H., Ahn, T., Noh, J., Yoon, S., Hwang, C., Seok, S., 2015. Efficient $CH_3NH_3PbI_3$ perovskite solar cells employing nanostructured p-type NiO electrode formed by a pulsed laser deposition. Adv. Mater. 27, 4013–4019.

Park, M., Lee, S., Kim, J., Kang, S., Kim, H., Choi, C., Ahn, K., 2014. Enhanced photoelectrochemical response of CdSe quantum dot-sensitized p-type NiO photocathodes. Phys. Status Solidi A 211, 1868–1872.

Peng, B., Tang, L., Zeng, G., Fang, S., Ouyang, X., Long, B., Zhou, Y., Deng, Y., Liu, Y., Wang, J., 2018. Self-powered photoelectrochemical aptasensor based on phosphorus doped porous ultrathin g-C_3N_4 nanosheets enhanced by surface plasmon resonance effect. Biosens. Bioelectron. 121, 19–26.

Peng, B., Lu, Y., Luo, J., Zhang, Z., Zhu, X., Tang, L., Wang, L., Deng, Y., Ouyang, X., Tan, J., Wang, J., 2021. Visible light-activated self-powered photoelectrochemical aptasensor for ultrasensitive chloramphenicol detection based on DFT-proved Z-scheme Ag_2CrO_4/g-C_3N_4/graphene oxide. J. Hazard. Mater. 401, 123395.

Peng, L., Hu, L., Fang, X., 2014. Energy harvesting for nanostructured self-powered photodetectors. Adv. Funct. Mater. 24, 2591–2610.

Shi, X., Wang, C., Zhu, Y., Zhao, W., Yu, X., Xu, J., Chen, H., 2018. 3D semiconducting polymer/graphene networks: toward sensitive photocathodic enzymatic bioanalysis. Anal. Chem. 90, 9687–9690.

Song, Z., Fan, G., Li, Z., Gao, F., Luo, X., 2018. Universal design of selectivity-enhanced photoelectrochemical enzyme sensor: integrating photoanode with biocathode. Anal. Chem. 90, 10681–10687.

Sreekumar, A., Poisson, L., Rajendiran, T., Khan, A., Cao, Q., Yu, J., Laxman, B., Mehra, R., Lonigro, R., Li, Y., Nyati, M., Ahsan, A., Kalyana-Sundaram, S., Han, B., Cao, X., Byun, J., Omenn, G., Ghosh, D., Pennathur, S., Alexander, D., Berger, A., Shuster, J., Wei, J., Varambally, S., Beecher, C., Chinnaiyan, A., 2009. Metabolomic profiles delineate potential role for sarcosine in prostate cancer progression. Nature 457, 910–914.

Suganya, M., Balu, A.R., 2017. PbS nanopowder-synthesis, characterization and antimicrobial activity. Mater. Sci. Pol. 35, 322–328.

Tang, L., Ouyang, X., Peng, B., Zeng, G., Zhu, Y., Yu, J., Feng, C., Fang, S., Zhu, X., Tan, J., 2019. Highly sensitive detection of microcystin-LR under visible light using a self-powered photoelectrochemical aptasensor based on a CoO/Au/g-C_3N_4 Z-scheme heterojunction. Nanoscale 11, 12198–12209.

Tong, W., Wang, Z., Wang, X., Zhang, X., Zhang, Y., An, Q., 2021. Self-powered materials obtained by interfacing functional assemblies with energy harvesting films. Mater. Chem. Front. 5, 2623–2648.

Wang, P., Cao, L., Chen, Y., Wu, Y., Di, J., 2019. Photoelectrochemical biosensor based on Co_3O_4 nanoenzyme coupled with PbS quantum dots for hydrogen peroxide detection. ACS Appl. Nano Mater. 2, 2204–2211.

Wang, Q., Yang, C., Yang, Q., Yu, S., Yang, H., 2019. Platinum-loaded mesoporous nickel phosphonate and its electrochemical application for sarcosine detection. Anal. Chim. Acta 1046, 93–98.

Wu, P., Liu, Z., Chen, D., Zhou, M., Wei, J., 2018. Flake-like NiO/WO_3 p-n heterojunction photocathode for photoelectrochemical water splitting. Appl. Surf. Sci. 440, 1101–1106.

Xu, X., Liu, Z., Zuo, Z., Zhang, M., Zhao, Z., Shen, Y., Zhou, H., Chen, Q., Yang, Y., Wang, M., 2015. Hole selective NiO contact for efficient perovskite solar cells with carbon electrode. Nano Lett. 15, 2402–2408.

Yang, X., Feng, X., Jin, X., Shao, M., Yan, B., Yan, J., Zhang, Y., Zhang, X., 2019. An illumination-assisted flexible self-powered energy system based on a Li–O_2 battery. Angew. Chem. Int. Ed. 58, 16411–16415.

Yang, Y., Zhang, W., Xu, Y., Sun, H., 2018. Preparation of PbS and CdS cosensitized graphene/TiO_2 nanosheets for photoelectrochemical protection of 304 stainless steels. Appl. Surf. Sci. 452, 58–66.

Yao, X., Gao, J., Yan, K., Chen, Y., Zhang, J., 2020. Ratiometric self-powered sensor for 17β-estradiol detection based on a dual-channel photocatalytic fuel cell. Anal. Chem. 92, 8026–8030.

Zeng, H., He, H., Fu, Y., Zhao, T., Han, W., Xing, L., Zhang, Y., Zhan, Y., Xue, X., 2018. A self-powered brain-linked biosensing electronic-skin for actively tasting beverage and its potential application in artificial gustation. Nanoscale 10, 19987–19994.

Zhang, L., Zhu, Y., Liang, Y., Zhao, W., Xu, J., Chen, H., 2018. Semiconducting CuO nanotubes: synthesis, characterization, and bifunctional photocathodic enzymatic bioanalysis. Anal. Chem. 90, 5439–5444.

Zhao, B., Wang, F., Chen, H., Zheng, L., Su, L., Zhao, D., Fang, X., 2017. An ultrahigh responsivity (9.7 mA W−1) self-powered solar-blind photodetector based on individual ZnO–Ga_2O_3 heterostructures. Adv. Funct. Mater. 27, 1700264.

Zhong, T., Li, H., Zhao, T., Guan, H., Xing, L., Xue, X., 2021. Self-powered/self-cleaned atmosphere monitoring system from combining hydrovoltaic, gas sensing and photocatalytic effects of TiO_2 nanoparticles. J. Mater. Sci. Technol. 76, 33–40.

Zhu, J., Nie, W., Wang, Q., Wen, W., Zhang, X., Li, F., Wang, S., 2020. A competitive self-powered sensing platform based on a visible light assisted zinc–air battery system. Chem. Commun. 56, 5739–5742.

Zhu, J., Luo, G., Peng, X., Wen, W., Zhang, X., Wang, S., 2021. Visible light mediated self-powered sensing based on target induced recombination of photogenerated carriers. J. Hazard. Mater. 407, 124765.

Zhu, T., Zhang, Y., Luo, L., Zhao, X., 2019. Facile fabrication of NiO-decorated double-layer single-walled carbon nanotube buckypaper for glucose detection. ACS Appl. Mater. Interfaces 11, 10856–10861.

Zhu, Y., Liu, Y., Xu, Y., Ruan, Y., Fan, G., Zhao, W., Xu, J., Chen, H., 2019. Three-dimensional TiO_2@Cu_2O@nickel foam electrodes: design, characterization, and validation of O_2-independent photocathodic enzymatic bioanalysis. ACS Appl. Mater. Interfaces 11, 25702–25707.